

# Experimental and Monte Carlo investigation of Visible Diffuse Reflectance Imaging sensitivity to diffusing particle size changes in an optical model of a Bladder Wall

Nina Kalyagina<sup>1,2</sup> · Viktor Loschenov<sup>1</sup> · Didier Wolf<sup>2</sup> · Christian Daul<sup>2</sup> · Walter Blondel<sup>2</sup> and · Tatiana Savelieva<sup>1</sup>

<sup>1</sup>Prokhorov General Physics Institute, Russian Academy of Sciences, 119991, Russia, Moscow, Vavilov Str, 38

<sup>2</sup>Centre de Recherche en Automatique de Nancy (CRAN UMR 7039), Nancy University, CNRS), 2 avenue de la forêt de Haye, 54516 Vandœuvre-Les-Nancy, France

**Abstract** We have investigated the influence of scatterers size changes on the laser light diffusion, induced by a collimated monochromatic laser irradiation, in tissue-like optical phantoms using diffuse reflectance imaging. For that purpose three-layer optical phantoms were prepared, in which nano- and microspheres size varied in order to simulate the scattering properties of healthy and cancerous urinary bladder walls. The informative areas of the surface Diffuse-Reflected light distributions were about  $15 \times 18$  pix for the smallest scattering particles of  $0.05 \mu\text{m}$ , about  $21 \times 25$  pix, for the medium-size particles of  $0.53 \mu\text{m}$ , and about  $25 \times 30$  pix for the largest particles of  $5.09 \mu\text{m}$ . The computation of the laser spot areas provided useful information for the analysis of the light distribution with high measurement accuracy up to 92%. The minimal stability of 78% accuracy was observed for superficial scattering signals on the phantoms with the largest particles. The experimental results showed a good agreement with the results obtained by the Monte Carlo simulations. The presented method shows a good potential to be useful for a tissue-state diagnosis of the urinary bladder.

## 1 Introduction

### 1.1 Formation of neoplasms

It is well known that malignant neoplasms of urinary bladder mainly arise in the inner urothelial layer of a bladder wall [1]. Usually, pathological stages of epithelial tissues, such as dysplasia or carcinoma *in situ*, precede cancer. Furthermore, on a microscopic visual aspect, dysplastic neoplasms do not differ much from the surrounding healthy tissue, which complicates the clinical diagnosis [2]. Main changes, associated to dysplasia, at a cellular level are: variations of the cell and nucleus shapes and sizes (increase of nuclear diameter), and hyperchromaticity [3]. Besides, sometimes non-malignant dysplastic cells show chaotic reproduction, which leads to the increase in population density [4].

White light (WL) cystoscopy is the standard clinical examination for *in vivo* bladder cancer detection. During cystoscopy, targeted and random biopsies are performed for histopathological analysis of tissue samples leading to final diagnosis. But the latter procedure has a poor sensitivity especially in the detection of invisible early precancerous tissue stages (limited number of “blind” biopsies) [3, 5, 6]. In many cases when an urothelial neoplastic lesion has been detected, because of its multi-focal nature [7], there is still a probability of unnoticed malignant focuses existence, up to 10% [5, 8], and of recurrence appearance, up to 70% [9]. Recent works have demonstrated the additional value of fluorescence cystoscopy in improving the contrast between healthy and tumoral tissues *in vivo* [10, 11]. By guiding more efficiently the biopsies, fluorescent cystoscopy combined to the WL provides diagnostic sensitivity increase (90% instead of 60% under the WL alone). However, these methods still suffer from low specificity [12, 13] due to high rates of false-positive results [5].

Complementary to the aforementioned fluorescence approach, the multiple diffusion of the light can be used to characterize tissue structure related to healthy and pathological stages [3]. In human tissues, the scattering process occurs due to the constituents of various size, concentration and refraction indices, and at different scales from cellular organelles to extracellular matrix compounds [2]. The smallest scatterers in the tissue are small cell organelles such as endoplasmic reticulum, component parts of Golgi apparatus, and individual fibers. Due to the sizes the scattering process on such tissue structures is described by the Rayleigh’s theory (1871). The sizes of mitochondria and lysosomes [4] can be compared to the wavelength of a visible range, while the nucleus diameter

is much bigger. However, their contribution to the scattering process can be described by the same theory which was first introduced by Gustav Mie in 1908 [14].

## 1.2 Visible Diffuse Reflectance Imaging

Non-polarized Diffuse Reflectance Imaging (DRI) is an approach which can be easily coupled to WL endoscopic imaging and provides additional information for a precancerous tissue diagnosis non-invasively. The principle of the DRI coupled to cytoscopy is to illuminate some areas on the tissue surface by means of the optical fibers, and to measure spatial distribution of the back-scattered non-polarized light. The backscattered light, arising from illuminated tissues, is influenced by the changes in nuclear size, epithelium thickness and other tissue components, thus is distributed according to the tissue structure.

As it was mentioned in the previous section, one of the main morphological features for differentiating precancerous tissues from healthy ones is the size of cell nuclei which are significantly enlarged in precancerous cells (higher nucleus-cytoplasm ratio) [3]. In this paper, we present an experimental investigation of the sensitivity of the DRI to detection of the spatial intensity responses of a monochromatic light backscattered by a multi-layered phantom with various sizes of diffusing particles.

## 1.3 Diffuse Reflectance profile

The spatial intensity profile measured from the Diffuse Reflectance (DR) Image acquired from a surface of a media with diffusing spheres of various diameters under the homogenous irradiation of the surface of a media is expected to be characterized in the following way: the amount of the photons outcoming from the central part of the illuminated area of a medium, is greater than the one from the surrounding area. As it is illustrated in Fig.1 a, b, zone ii,  $p(x)$  along the adjoining area (i.e. a decreasing amount of diffusively back-reflected photons) decreases due to the multiple scattering and absorption inside the tissue, whereas the photons are mainly directly back-reflected in the central part of the illuminated spot, because of a specular reflection of the incident light. By comparing the intensity profiles, showed in the Fig. 1a and 1b, for small and large diameters of diffusing particles in the medium, one can see that the central zones (i) are equivalent, unlike the lateral zones (ii) which differ with the scatterer diameters.

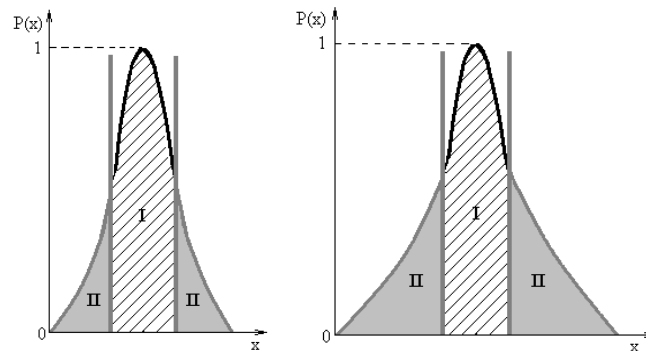


**Fig. 1a,b** Probability spatial distribution profile of DR light at the surface of irradiated media (a) with small (50 nm - 200 nm) particles, (b) with bigger (500 nm - 5  $\mu$ m) particles

## 2 Materials and Methods

### 2.1 Phantom construction

Phantoms simulating the optical behaviour of urinary bladder wall can be useful to understand the mechanism of internal light scattering and to identify the main features in differences of DR light signals.

Multilayered synthetic phantoms of three types were constructed by means of superposition of three layers. Each layer, simulating different parts of the urinary bladder wall, had different thickness and optical properties.

The first layers varied in sizes of diffusing particles, while the two others were identical for all types of the phantoms.

The first (top) layer simulated diffusing optical properties of cell nuclei of transitional epithelium of the urinary bladder mucosa. A substance, made from gelatine powder of 5% concentration and micro and nano polystyrene spheres suspended in distilled water, was taken as a basic component of the medium. The polystyrene spheres are classically used to simulate scattering properties of biological tissues [15]. To estimate the contribution of different size of the scatterers to the scattering process inside the medium, the microspheres of various diameters in a concentration of  $10^7$  spheres per ml were used as main scatterers of the first layers of the phantoms. The particles of the smallest diameter of 50 nm were added to the phantoms of a 1<sup>st</sup> type, the microspheres of 0.53  $\mu\text{m}$  diameter - to the phantoms of a 2<sup>nd</sup> type, and the microspheres of 5.09  $\mu\text{m}$  diameter – to the phantoms of a 3<sup>rd</sup> type. The thickness of the first layers was 200  $\mu\text{m}$ .

The second and the third layers were made from Intralipid in 1.6% and 2.0% concentrations, respectively, and of gelatine powder of 5% concentration, diluted in distilled water. The thickness of the second layers was 700  $\mu\text{m}$ , and of the third - 2100  $\mu\text{m}$ . All layers were put into a Petri dish with a coloured black bottom for the absorption.

To estimate the contribution of the directly-reflected light to the surface light distribution on the models we have calculated the refractive indices  $n$  for all types of the phantoms, using the law of Gladstone and Dale [16]:

$$n = n_1 c_1 + n_2 c_2, \quad (1)$$

where  $n_1$ ,  $n_2$  and  $c_1$ ,  $c_2$  are the refractive indices and volume fractions of a substance (gelatin matrix and water) and scattering particles respectively, and  $c_1 + c_2 = 1$ . Such reflection in a couple with the DR, accumulated in the central area near the incident beam, forms the area  $i$  in the Fig.1.

The refractive index of the polystyrene particles is  $n_p=1.59$  [17]. The substance of the first layers, surrounding the scattering particles, consists of gelatin particles with  $n_{gel}=1.533$ , and of water, with

$$n_{wat} = 1.31848 + \frac{6.662}{\lambda[nm]-129.2} \quad (2)$$

for the wavelength of 532 nm [18]. Thus, the refractive index of the surrounding medium of the first layers is

$$n_{1med} = 0.05n_{gel} + 0.95n_{wat} \quad (3)$$

The full refractive indices of the first layers with the particles of 0.05  $\mu\text{m}$  and 0.53  $\mu\text{m}$  diameter are equal to the index of the surrounding medium, as the impact of the spheres to the refractive indices can be neglected due to the low volume fractions, which are  $6.5 \times 10^{-10}$  and  $7.8 \times 10^{-7}$ , respectively. The refractive index of the first layer with the particles of 5.09  $\mu\text{m}$  diameter is:

$$n_{1,5.09} = 6.9 * 10^{-4} n_{sph} + 0.9993 n_{1med} \quad (4)$$

The indices of refraction of the second and the third layers of our models are calculated in consideration of the refractive index of Intralipid 20% ( $n_{int20\%}=1.361$  for the 532 nm wavelength [19]):

$$n_{2med} = 0.016n_{int100\%} + 0.05n_{gel} + 0.934n_{wat} \quad (5) \text{ and}$$

$$n_{3med} = 0.02n_{int100\%} + 0.05n_{gel} + 0.93n_{wat} \quad (6)$$

The Fresnel reflection of the light entering the medium is [20]:

$$R = \left( \frac{1-n}{1+n} \right)^2 \quad (7)$$

Thus the Fresnel reflections for our mediums with different scattering particles are:  $R_{0.05} = 0.0216$  (2.2%),  $R_{0.53} = 0.0216$  (2.2%), and  $R_{5.09} = 0.0217$  (2.2%)

## 2.2 Experimental set-up

See full version

## 2.3 Monte Carlo modelling

See full version

**Table 1** The input parameters for the Monte Carlo modelling

Name/ Parameter	refractive index, n	anisotropy factor, g	scattering coefficient, $\mu_s$ , [cm-1]	absorption coefficient, $\mu_a$ , [cm-1]
First layer with the spheres of 0.05 $\mu\text{m}$	1.3449	0.027	0.000015	0.001
First layer with the spheres of 0.53 $\mu\text{m}$	1.3449	0.867	0.024	0.001
First layer with the spheres of 5.09 $\mu\text{m}$	1.34505	0.87	3.9	0.001
Second layer	1.347	0.79	10	0.001
Third layer	1.34752	0.79	15	0.001

## 3 Image processing

### 3.1 Image subtraction

See full version

### 3.2 Three-dimensional diagrams

See full version

The experimental results were compared with simulated results obtained in the MC program. The matrices of the DR light on the tissue were processed in a MATLAB program in order to visualise the light distributions on the surfaces of the models (Fig.6). The received signals were normalised according to the quantity of the back-scattered photons between 0 and 1, where 0 corresponds to the lowest quantity of the photons, hit the surface, and 1 corresponds to the highest quantity of the photons, hit the surface. For the  $10^7$  of initialized photons and  $10^7$  packets of photons the lower threshold was  $10^8$  photons, and the upper was  $3 \times 10^{10}$  photons.

The images of the simulated diffusive light distribution show a similar character to the experimental ones: the highest intensities of the DR light were on the surfaces of the phantoms with the largest particles of 5.09  $\mu\text{m}$ , unlike the lowest intensities on the surfaces of the phantoms with the smallest particles of 0.05  $\mu\text{m}$ .

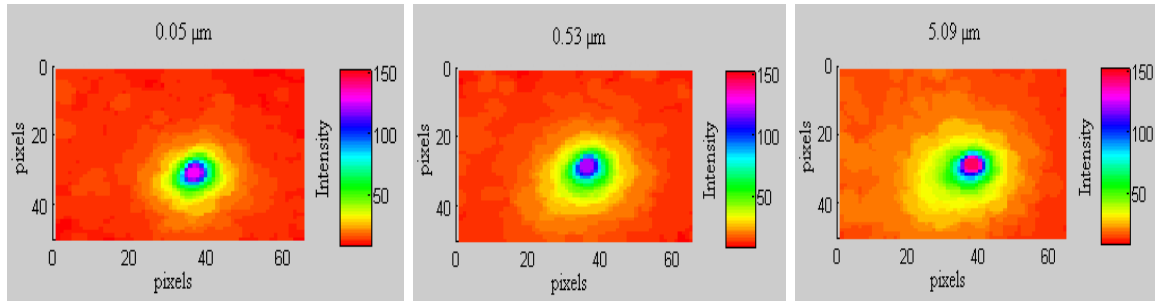


**Fig. 5a, b, c** 3-D intensity diagrams of the Diffuse-Reflected light from the particles of different diameter: (a) 50 nm, (b) 0.53  $\mu\text{m}$ , (c) 5.09  $\mu\text{m}$

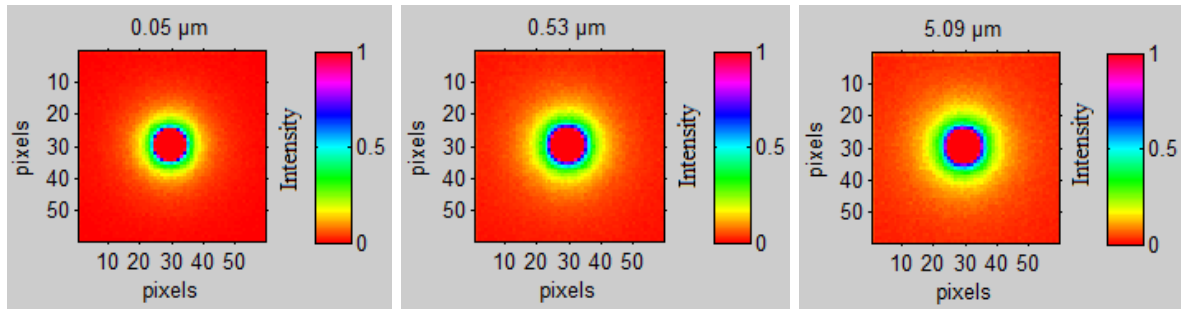


**Fig. 6** Modelled images of the Diffuse-Reflected light on the surfaces of the phantoms in a hue, saturation and intensity value colour space for the particles of different diameter: (a) 50 nm, (b) 0.53  $\mu\text{m}$ , (c) 5.09  $\mu\text{m}$

### 3.3 Area measuring

However, obtaining only visual information was not satisfying enough. To quantify the differences in the patterns, the correlation between the diameters of spheres and the area of DR light in the image field were calculated.

To perform such calculus the initial truecolor RGB images (with pixel values from 0 to 255) were first converted to the grayscale ones (with pixel intensity values from 0 to 1), and then to binary, where all pixels have had only two possible values 0 and 1. Each image was divided into foreground and background pixels, creating two sets:

$$\begin{aligned} G_1 &= \{f(m,n): f(m,n) > t\} \text{ (foreground pixels)} \\ G_2 &= \{f(m,n): f(m,n) \leq t\} \text{ (background pixels)} \end{aligned} \quad (12)$$

where  $f(m,n)$  is the value of pixel located in the  $m^{\text{th}}$  column,  $n^{\text{th}}$  row [33], and  $t$  is a threshold value.

Symmetrically chosen values  $x_1$  and  $x_2$  in the zones ii on axis  $x$  (Fig. 1), give us the two extreme points of the back-scattering areas, so that the value  $d = |x_2 - x_1|$  corresponds to the diameter of the areas. The threshold value 0.11 for the grayscale images lies near the border of the DR light on the surfaces of the phantoms, thus it was chosen to measure the DR area values. Therefore all pixels with luminance, greater than 0.11, were replaced with 1 (the white colour), and the values of all other pixels were replaced with 0 (the black colour).

Such operation has allowed us to get the numerical results and to measure the necessary areas equal to the halo diameters. For the higher calculation accuracy we have filled in all the holes which were remaining in the black images area after their conversion to the binary format. Then, to receive the area values, the total of the “white” areas with the pixel value 1 was calculated for each binary image (Fig. 7).

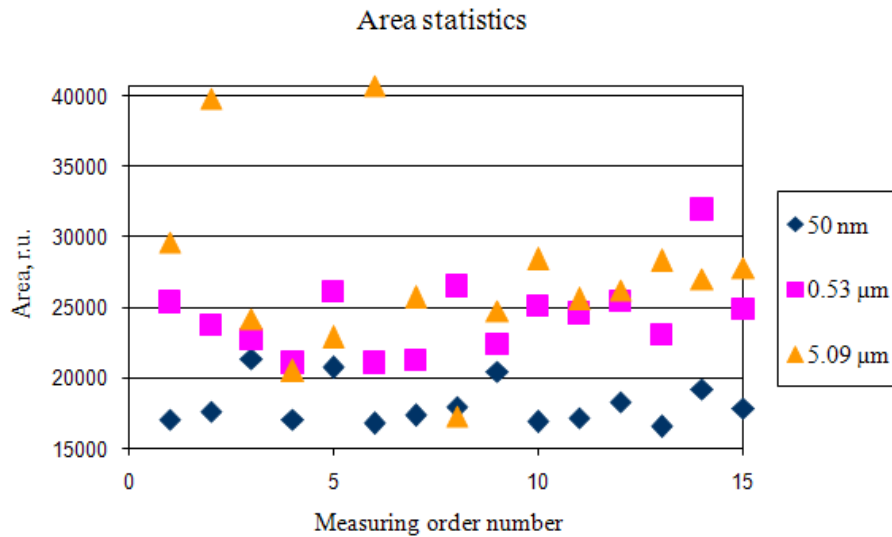


**Fig. 7** Distribution of the area values for the Diffuse-Reflected light from the phantoms with the particles of 50 nm diameter (◆), 0.53 μm (■), and 5.09 μm (▲)

We have processed 45 images of DR light on a surface of the irradiated phantoms (15 images for each type of the phantom), thus the probability of each event was 1/15. To calculate the standard mean-square errors we have calculated the variances of the expected values, and, by square-rooting, the standard deviations for the areas with light intensity higher than 0.11 for each binary image (Table 2). The variance of the expected value of the DR light area is equal to the mean of the square minus the square of the mean:  $E(X) = \sum_{i=1}^{15} x_i * p(x_i)$ , where  $x_i$  - the area value,  $X$  - is a mean value of the area,  $E(X)$  - expected value,  $p(x_i)$  - probability of an area value. The variance of the expected value is [34]:  $var(X) = E[X^2] - (E[X])^2$ .

See full version

The area measurements have provided us with the information on the laser spot diameter with a high accuracy 89-92% (Table 2). However a higher standard deviation for the microparticles of 2<sup>nd</sup> and 3<sup>rd</sup> type (see Section 2.1) is seen. The anisotropy factors of the particles of 0.53 μm and 5.09 μm in a concentration of  $10^7$  are very similar to each other (Table 1), and their high values move the photons strongly lower and make them hit the next scatterers faster. The scattering coefficients of the biggest particles of the media are about 160 times higher than of the medium size and about  $2.6 \times 10^5$  times higher than of the smallest, which reduces the mean free path between the two acts of the scattering event in the media with the particles of 5.09 μm diameter. Thereafter such particular differences in the scattering properties of the media explain the more obvious differences in the DR signals between the particles of 0.05 μm and 0.53 μm. Nevertheless, the distinctive features of light beams, back-scattered by microparticles of big diameters (0.53 μm and 5.09 μm), in their shape, size and intensity, are seen (Table 2).

**Table 2** Parameters calculated for the areas of Diffuse-Reflection

Diameter of polymer spheres/ Measures parameters	50 nm	0.53 $\mu\text{m}$	5.09 $\mu\text{m}$
Mean area	18170.8	24356.9	27266.3
Variance of expected value	2259021	7176856.1	35561233
Standard deviation	1503	2679	5963
Accuracy	92%	89%	78%

#### 4 Conclusion

The presented method describes a technique for detection of the differences in the surface back-scattered light signals from the media with different diameters of the scatterers. The obtained results reveal a contribution of polymer particles of different sizes to the light diffusion in biological models of the urinary bladder wall. Development of the image processing methods has provided us with the extraction of the DR parameters, which makes possible the differentiation between the back-reflected light from the particles of 50 nm, 0.53  $\mu\text{m}$  and 5.09  $\mu\text{m}$  diameters.

The results show that the DRI method has a high potential to be useful for *in vivo* diagnosis of urinary bladder. The greater impact to the scattering process is made by the particles of the bigger diameter of 5.09  $\mu\text{m}$ , which is in a good conformity with the sizes of a cell nucleus, in which main initial cancerous transformations arise. The impact of the other scatterers to the DR signal can be used for estimation of the background signal, that does not change during the cancerous transformations, and may be subtracted, or considered as a zero signal. However the accuracy (78%) of the measured areas of back-scattered light for the phantoms with the scattering particles of 0.53  $\mu\text{m}$  and 5.09  $\mu\text{m}$  diameters, in the concentration of  $10^7$  spheres per ml, is relatively low. The increase in the concentration of the scatterers and augmentation of the quantity of the measurements will lead to the increase of the accuracy and sensitivity of the method due to the strong differences in the scattering parameters. To enhance the potential of the diagnostic optical system and to avoid measurement errors, several addition fiber-optical laser channels can be added to the existing set-up.

Moreover for the further analysis it is necessary to take into account some other aspects of the neoplasmes formation, such as chromaticity changes and population density changes, which strongly influence the absorption and scattering properties. Such kind of studies can provide useful information on the tissue state and may be applied for the clinical uses. The results of MC modelling, obtained by varying the input parameters of the under investigation medium, can serve as a calibration for the presented method.

**Acknowledgements** The work has been supported by the Ministry of Education and Science of the Russian Federation within the framework of the National Program “Scientific and Scientific-educational Personnel of the Innovative Russia (2009-2013)” (Contract No. P544).

#### References

1. V. Backman, M. Wallace, L. Perelman, J. Arendt, R. Gurjar, M. Müller, Q. Zhang, G. Zonios, E. Kline, J. McGilligan, S. Shapshay, T. Valdez, K. Badizadegan, J. Crawford, M. Fitzmaurice, S. Kabani, H. Levin, M. Seiler, R. Dasari, I. Itzkan, J. Van Dam, M. Feld: *Nature* 406 (2000)

2. V. Tuchin, *Optical Biomedical Diagnostics 2* (Fizmalit, Moscow 2007)
3. R. Gurjar, V. Backman, L. Perelman, I. Georgakoudi, K. Badizadegan, I. Itzkan, R. Dasari, M. Feld: *Nature Medicine* 7, 11 (2001)
4. V. Backman: *Imaging human epithelial properties with polarized light scattering spectroscopy* (PhD Thesis 2001)
5. N. Nese, R. Gupta, M. Bui, M. Amin.: *J. Natl. Compr. Canc. Netw.* 7, 1 (2009)
6. M. Babjuk: *European Urology Supplements* 8 (2009)
7. T. Kakizoi: *Cancer Sci.* 97, 9 (2006)
8. B. Tetu: *Modern Pathology* 22 (2009)
9. M. Ihnat, K. Kyker, J. Thorpe, S. Shenoy, R. Hurst: *American Journal of Pharmacology and Toxicology* 1, 4 (2006)
10. T. Filbeck, U. Pichlmeier, R. Knuechel, W. Wieland, W. Roessler: *Urology* 60, 6 (2002)
11. D. Barocas, P. Clark: *Curr. Opin. Oncol.* 20, 3 (2008)
12. E. Cauberg, D. de Bruin., D. Faber, T. van Leeuwen, J. de la Rosette, T. de Reijke: *European Urology* 56 (2009)
13. A. Stenzl, S. Kruck: *Expert Rev. Anticancer Ther.* 9, 6 (2009)
14. C. Bohren, D. Huffman: *Absorption and scattering of light by small particles* (A Wiley-Interscience Publication John Wiley & Sons, New-York 1998)
15. R. Studinski, I. Vitkin: *J. Biomed. Opt.* 3, 5 (2000)
16. J. Gladstone, T. Dale: *Phil. Trans. Royal Soc. London* 153 (1864)
17. Bang Laboratories: *TechNote 100 (Polymer Microspheres)* (2010)
18. A. Bashkatov, E. Genina, V. Kochubey, V. Tuchin: *Proceedings of SPIE* 3917 (2000)
19. H. Ding, J. Lu, K. Jacobs, X-H Hu: *J. Opt. Soc. Am. A* 22, 6 (2005)
20. E. Hecht: *Optics*, 4 ed. (Addison Wesley 2002)
21. H. van Staverent, J. Beeu, J. Ramaekerst, M. Keijzerg, W. Star: *Phys. Med. Biol.* 39 (1994)
22. T. Beck, W. Beyer, T. Pongratz, W. Stummer, R. Waidelich, H. Stepp, S. Wagner, R. Baumgartner: *Proceedings of SPIE-OSA Biomedical Optics*, SPIE 5138 (2003)
23. L. Wang, S. Jacques, L. Zheng: *Comp. Meth. in Biomed.* 47 (1995)
24. C. Palmer, N. Ramanujam: *Appl. Opt.* 5, 45 (2006)
25. Z. Matuszak, A. Sawow, M. Wasilewska-Rdwanska: *Pol. J. Med. Phys. Eng.* 4, 10 (2004)
26. M. Quinten, J. Stier: *Colloid and Polym. Sci.*, 272 (1995)
27. H. Kang, J. Kim, Y. Yu, J. Oh: *Journal of the Korean Physical Society* 55, 5 (2009)
28. C. Amra: *Applied Optics* 32, 28 (1993)
29. T. Lehmann, C. Gonner, K. Spitzer: *IEEE Transactions on Medical Imaging* 18, 11 (1999)
30. M. Póth, T. Szakáll: *10th International Symposium of Hungarian Researchers on Computational Intelligence and Informatics* (2009)
31. E. Maeland: *IEEE Trans. Med. Imag.*, MI-7 (1988)
32. R. Jones, I. Svable: *IEEE Transactions on Pattern Analysis and Machine Intelligence* 16, 6 (1994)
33. L. Shapiro, G. Stockman: *Computer Vision* (Upper Saddle River, NJ: Prentice-Hall 2001)
34. V. Gmurman, I. Berenblut: *Fundamentals of Probability Theory and Mathematical Statistics* (American Elsevier Pub. Co., New York 1968)
35. R. Fisher (1925): *Statistical Methods for Research Workers*, first ed. (Edinburgh: Oliver & Boyd 1925)